EINDHOVEN UNIVERSITY OF TECHNOLOGY

Ultra-thin aluminium oxide films deposited by plasma-enhanced atomic layer deposition for corrosion protection

Citation for published version (APA):
Potts, S. E., Schmalz, L., Fenker, M., Díaz, B., Swiatowska, J., Maurice, V., Seyeux, A., Marcus, P., Radnóczi, G., Tóth, L., & Kessels, W. M. M. (2011). Ultra-thin aluminium oxide films deposited by plasma-enhanced atomic layer deposition for corrosion protection. *Journal of the Electrochemical Society*, *158*(5), C132-C138. https://doi.org/10.1149/1.3560197

DOI:
10.1149/1.3560197

Document status and date:
Published: 01/01/2011

Document Version:
Publisher’s PDF, also known as Version of Record (includes final page, issue and volume numbers)

Please check the document version of this publication:

• A submitted manuscript is the version of the article upon submission and before peer-review. There can be important differences between the submitted version and the official published version of record. People interested in the research are advised to contact the author for the final version of the publication, or visit the DOI to the publisher's website.
• The final author version and the galley proof are versions of the publication after peer review.
• The final published version features the final layout of the paper including the volume, issue and page numbers.

Link to publication

General rights
Copyright and moral rights for the publications made accessible in the public portal are retained by the authors and/or other copyright owners and it is a condition of accessing publications that users recognise and abide by the legal requirements associated with these rights.

• Users may download and print one copy of any publication from the public portal for the purpose of private study or research.
• You may not further distribute the material or use it for any profit-making activity or commercial gain
• You may freely distribute the URL identifying the publication in the public portal.

If the publication is distributed under the terms of Article 25fa of the Dutch Copyright Act, indicated by the “Taverne” license above, please follow below link for the End User Agreement:

www.tue.nl/taverne

Take down policy
If you believe that this document breaches copyright please contact us at:

openaccess@tue.nl

providing details and we will investigate your claim.

Download date: 23. Aug. 2022

Journal of The Electrochemical Society, **158** (5) C132-C138 (2011)
0013-4651/2011/158(5)/C132/7/$28.00 © The Electrochemical Society

Ultra-Thin Aluminium Oxide Films Deposited by Plasma-Enhanced Atomic Layer Deposition for Corrosion Protection

S. E. Potts,[a,*,z] L. Schmalz,[b] M. Fenker,[b] B. Díaz,[c] J. Światowska,[c] V. Maurice,[c] A. Seyeux,[c] P. Marcus,[c] G. Radnóczi,[d] L. Tóth,[d] and W. M. M. Kessels[a,*,z]

[a]*Department of Applied Physics, Eindhoven University of Technology, 5600 MB Eindhoven, The Netherlands*
[b]*FEM Research Institute, Precious Metals & Metals Chemistry, 72525 Schwäbisch Gmünd, Germany*
[c]*Laboratoire de Physico-Chimie des Surfaces, CNRS (UMR 7045), École Nationale Supérieure de Chimie de Paris (Chimie ParisTech), 75005 Paris, France*
[d]*Research Institute for Technical Physics and Materials Science, H-1525 Budapest, Hungary*

We have employed plasma-enhanced and thermal atomic layer deposition (ALD) within the temperature range of 50–150°C for the deposition of ultra-thin (10–50 nm) Al_2O_3 films on 100Cr6 steel and aluminium Al2024-T3 alloys. $[Al(CH_3)_3]$ was used as the precursor with either an O_2 plasma or water as co-reactants. Neutral salt spray tests showed that the thicker films offered the best corrosion-resistance. Using cyclic voltammetry, the 50 nm films were found to be the least porous (<0.5%). For 10 nm thick films, plasma-enhanced ALD afforded a lower porosity and higher film density than thermal ALD. ToF-SIMS measurements on 100Cr6 showed that the main 'bulk' of the films contained very few impurities, but OH and C were observed at the interfaces. TEM confirmed that the films were conformal on all substrates and the adhesion was excellent for the films deposited by plasma-enhanced ALD but not for thermal ALD, as delamination was observed. On the basis of these and other results, the prospects of the application of ALD films for corrosion protection, and the use of plasma-enhanced ALD to promote their nucleation, is discussed.
© 2011 The Electrochemical Society. [DOI: 10.1149/1.3560197] All rights reserved.

Manuscript submitted November 19, 2010; revised manuscript received January 27, 2011. Published March 23, 2011.

Corrosion is a persistent problem for many modern high-precision applications, such as automotive[1] and aerospace[2–4] or speciality gas handling.[5–8] Components for these applications require many high-purity precision parts and instruments, which are commonly manufactured from steel or aluminium alloys. As such, these parts need to be protected by dense and defect-free coatings to prevent corrosion. Ideally, the coatings should be ultra-thin and form a complete sealing barrier to prevent contact between the alloy substrates and the surrounding electrolytes or corrosive gases in the environment. Deposition methods used for such films have included physical vapour deposition (PVD)[9,10] and chemical vapour deposition (CVD).[11,12] In particular, plasma-assisted CVD has been of interest,[13–15] as this allows for deposition at temperatures lower than are typical for CVD, which is beneficial when the substrates are temperature-sensitive, such as heat-treated industrial alloys.

Atomic layer deposition (ALD) is potentially an ideal candidate for this thin (<100 nm) film application, as it gives high-quality films with excellent conformality, and provides precise thickness control,[16] which arises from the sequential alternate dosing of metal halide or organometallic and non-metal precursors. For metal oxides, water and ozone are popular co-reactants, but recently oxygen plasmas have seen greater potential because of the presence of reactive ionic and radical species therein. The radicals in a plasma provide higher surface reactivity than is possible with thermal energy alone,[17–19] which allows for depositions at lower substrate temperatures, even down to room temperature.[20] This is crucial for temperature-sensitive substrates, such as heat-treated mild steel, for example. Also, the presence of ions can lead to mild bombardment of the film (depending on the plasma configuration and conditions),[18] which contributes to increased density[19] and can thereby potentially improve the sealing performance of the coatings. An additional benefit of plasma-enhanced ALD is that a higher density of reactive surface groups are obtained compared with thermal ALD.[21] This, in turn, can lead to the higher growths per cycle; for example, van Hemmen et al. reported a growth per cycle at 150°C of 0.12 nm/cycle for Al_2O_3 from $[Al(CH_3)_3]$ and an O_2 plasma,[22] whereas where water was the oxygen source, the growth per cycle was 0.09 nm/cycle in the same reactor.

* Electrochemical Society Active Member.
z E-mail: s.e.potts@tue.nl; w.m.m.kessels@tue.nl

Thermal ALD has been employed as a method for depositing corrosion-resistant metal oxide layers onto stainless steel[23] and aluminium,[24] which improved the substrates' resistance to acidic and alkaline solutions, respectively. Additionally, the feasibility of layers deposited by ALD as barrier materials has been demonstrated on organic polymer substrates, which also require low deposition temperatures, for use in organic LEDs.[25–28] It was shown that Al_2O_3 deposited by ALD using water,[25,26] ozone[27] and an O_2 plasma[28] as the co-reactant could be used to deposit thin films which sealed the substrate. Langereis et al. reported that plasma-enhanced ALD gave Al_2O_3 with excellent sealing properties, where the films deposited at room temperature afforded the lowest water vapour transmission rate.[28] Despite this, to our knowledge, plasma-enhanced ALD has not been employed for the coating of metal alloys for corrosion protection. As such, the primary focus of this article aims to assess the suitability of Al_2O_3 deposited by plasma-enhanced ALD, from $[Al(CH_3)_3]$ with an O_2 plasma, as a protective layer for 100Cr6 mild steel and aluminium Al2024-T3 alloys, in comparison with thermal ALD (using water as the oxygen source).

Experimental

Atomic layer deposition.—The experiments were carried out on a commercially-built Oxford Instruments OpAL reactor located in a clean-room. It is an open-load system, which operates with a rotary pump. The base pressure was ~1 mTorr and typical operating pressures were 100–1000 mTorr. Trimethylaluminium, $[Al(CH_3)_3]$ (AkzoNobel, purity >99.9%,) was employed as the aluminium precursor and was held in a stainless steel bubbler at 24°C. Oxygen and argon (both purity >99.999%) were flowed into the reaction chamber at 50 and 20 sccm, respectively, throughout the plasma-enhanced ALD process. Argon alone was used to purge the precursor lines. The substrate temperature was 50, 100 or 150°C. For the thermal ALD process, water (VWR, GBR Rectapur grade, >99.999%) was also held in a water-cooled stainless steel bubbler at 19°C to reduce the vapour pressure and prevent overdosing. Only argon (200 sccm) was used as a process gas for the thermal ALD experiments and 150°C was the only substrate temperature employed. The cycle times ($[Al(CH_3)_3]$ – purge – co-reactant – purge) are as follows: plasma-enhanced ALD, 0.05–5–4–2 s; thermal ALD, 0.05–5–0.02–10 s. For all ALD processes, the parameters are outlined in Table I. The number of cycles chosen to obtain the

Downloaded 29 Mar 2011 to 131.155.151.8. Redistribution subject to ECS license or copyright; see http://www.ecsdl.org/terms_use.jsp

Table I. The experimental conditions used, and the film thicknesses and refractive indices measured using spectroscopic ellipsometry (SE) on an n-type Si substrate.

ALD method	Deposition temperature (°C)	Number of ALD cycles	Nominal thickness (nm)	SE thickness on Si (±0.05 nm)	SE refractive index at 630 nm (±0.02)
Plasma-enhanced	50	55	10	10.3	1.56
—	100	69	10	11.0	1.57
—	150	76	10	10.9	1.58
—	150	151	20	20.6	1.58
—	150	385	50	50.9	1.62
Thermal	150	112	10	10.9	1.58
—	150	556	50	54.0	1.61

desired film thicknesses was based on the growths per cycle reported previously in our earlier work (plasma-enhanced ALD: 0.16, 0.14, and 0.13 nm/cycle at 50, 100, and 150°C, respectively; thermal ALD with water: 0.09 nm/cycle at 150°C).[20,22]

Substrates.— 100Cr6 steel (Schäffler) and Al2024-T3 aluminium (Messier-Bugatti) alloys were employed as substrates. For the 100Cr6, fine-ground and lapped surface preparations were investigated and the Al2024-T3 samples had a fine-ground surface finish. The fine-ground surface finish was obtained using a planar grinding machine (Kehren, type RS) using corundum (Tyrolit, 89A461H9AV2) as a grinding medium with lubricant (Hosmac 928). The lapped surface finish was obtained upon further treatment of the fine-ground surfaces using an Elap 400 machine with a water-based diamond suspension (~6 μm, LamPlan Diamant MM342) for 2 h. After preparation, the substrates were dried in compressed nitrogen (99.999%) and coated in silicon oil (Sigma-Aldrich GmbH, no. 85409). Prior to transportation, the samples were packaged in membrane boxes (Inca S. A. Plastic) to prevent excess movement. Coated samples were also sent in the membrane boxes for analysis. Before deposition, the required substrates were cleaned in an ultrasonic isopropanol (Emplura grade, Merck Chemicals International) bath for 5 min and then blow-dried in room-temperature nitrogen. Reference substrates were used in each process, which were 1/4 100 mm n-type Si(100) wafers. These wafers were covered with a thin native oxide (SiO_2, ~1.5 nm) layer and did not undergo any additional cleaning steps.

Spectroscopic ellipsometry (SE).— A J. A. Woollam Inc. M2000 rotating compensator ellipsometer on a multi-angle Gonio stage (angles used: 65, 70, 75, and 80°) was employed to confirm the thickness and refractive index of the films on the reference Si substrates. Modelling was carried out using CompleteEASE software. The model layers comprised Si, native SiO_2 and Al_2O_3. The Al_2O_3 layer was modelled using a Cauchy layer over the wavelength range of 190–1000 nm (1.2–6.5 eV). Further details on the SE technique and modelling can be found in the literature.[29]

Electrochemical tests.— All electrochemical tests were performed using a 3-electrode system with a Pt counter electrode and a SCE reference electrode at ambient temperature (~20°C). The electrolytes were 0.5 M NaCl for the Al2024-T3 substrates and 0.2 M NaCl for the 100Cr6 substrates, prepared with ultra-pure water (resistivity >18 MΩ cm) and reagent grade chemicals (NaCl Analar Normapur analytical reagent VWR BDH Prolabo). These solutions were de-aerated by bubbling argon gas through them for 30 min prior to the measurements. The *p*H was 7.2 ± 0.2 prior to the corrosion test. The CV tests were performed afterwards from a cathodic vertex and in a potential range depending on the substrate and its susceptibility to pitting corrosion. All CV curves (including the reverse cathodic scan) were obtained at a scan rate of 1 mV s^{-1}. The electrochemical measurements on 100Cr6 substrates were performed on polished samples and Al2024-T3 substrates on fine-ground surfaces.

Transmission electron microscopy (TEM).— TEM analysis was carried out using a 200 kV Philips CM20 analytical TEM equipped with an EDS detector. Prior to the analysis, all samples were thinned by a standard mechanical grinding/ion bombardment technique. This involved cutting the substrates, embedding them into a custom-made Ti-holder, mechanical grinding and polishing, followed by 10 keV Ar ion milling. The final step was carried out at lower ion energy of 3 keV in order to decrease the surface damage of the thinned TEM specimens.

Time-of-flight secondary ion mass spectrometry (ToF-SIMS).— Elemental depth profiles were obtained using a ToF-SIMS 5 spectrometer (IonTof). The spectrometer was run at an operating pressure of 10^{-9} mbar in HC-BUNCHED mode. A pulsed 25 keV Bi^+ primary ion source was employed for analysis, delivering 1.8 or 0.86 pA of current over a 175×175 μm or 100×100 μm area for the 50 and 10 nm thick coatings, respectively. Depth profiling was performed using a 2 keV sputter beam giving a 100 or 82 nA target current over a 400×400 μm or 1000×1000 μm area for the 50 and 10 nm thick coatings, respectively. Data acquisition and post-processing analyses were performed using the Ion-Spec software. The profiles were recorded with negative secondary ions, which are more sensitive to fragments originating from oxide matrices.

Neutral salt spray (NSS) testing.— Neutral salt spray tests were performed according to the standard DIN 50021, ISO 9227 but with the deviation that the samples were rinsed in deionised water and dried with a hair dryer (warm, not hot air) before photographs were taken of the samples. The electrolyte was 50 ± 5 g L^{-1} (~0.86 M) NaCl with a *p*H value in the range of 6.5–7.2. The tests were carried out at a temperature of 35 ± 2°C. Photographs were taken of the samples after 2, 4, and 24 h testing. If no, or only negligible, corrosion products were visible, the samples were transferred back to the salt spray test chamber and the test was continued until significant red rust was visible on the 100Cr6 steel samples or white rust on the Al2024-T3 substrates, after which the samples were removed from the test chamber.

Results and Discussion

Al_2O_3 films were deposited on industrial alloys using plasma-enhanced and thermal ALD. For the coatings deposited by plasma-enhanced ALD, the corrosion characteristics were tested by conducting a thickness series of films of nominally 10, 20, and 50 nm on lapped 100Cr6 steel and fine-ground Al2024-T3 substrates at a deposition temperature of 150°C. Additionally, a temperature series was carried out at temperatures of 50, 100 and 150°C, focussing on 10 nm thick films. Higher temperatures could not be used due to the heat-treatment of the steel. Coatings deposited by thermal ALD (at 150°C only) with thicknesses of 10 and 50 nm were deposited on 100Cr6 and Al2024-T3 for comparison with the plasma-enhanced process.

The film thicknesses and refractive indices, measured by SE, are outlined in Table I. These measurements were taken from the n-type Si reference substrate included in the reaction chamber during the depositions. For the samples deposited by plasma-enhanced ALD,

Downloaded 29 Mar 2011 to 131.155.151.8. Redistribution subject to ECS license or copyright; see http://www.ecsdl.org/terms_use.jsp

the thicknesses were measured to be within 1 nm of the nominal thickness, while for the 50 nm thick film for thermal ALD, the thickness was ∼4 nm higher than intended. The refractive indices increased slightly with increasing film thickness and deposition temperature, suggesting a better bulk quality material. This is confirmed by previously-reported Rutherford backscattering results, which showed that films deposited at higher temperatures had higher densities,[20] which was attributed to there being a lower concentration of OH groups in those films.

CV porosity.—The porosity, which can be thought of as the percentage of uncoated film surface, was measured by cyclic voltametry.[30] For the films deposited by plasma-enhanced ALD on 100Cr6, the porosity was highest for the thinnest films, at ∼0.6%, with the porosity decreasing with increasing thickness to 0.07% for 50 nm thick films (see Fig. 1a). Where thermal ALD was used, the porosity was an order of magnitude higher for the 10 nm films, suggesting that nucleation and film densification was not as efficient using this process, leaving 3.65% of the 100Cr6 surface uncoated. The case was seemingly reversed for the 50 nm films, although the porosity of the films deposited using thermal ALD varied greatly over the samples, as shown by the error bar; therefore, the porosities of the films deposited by the two techniques were considered equivalent at a thickness of 50 nm. The thicker films have a higher probability of covering surface features more efficiently due to the greater amount of material being deposited. This thickness dependence could possibly be resolved by using a surface pre-treatment.

On Al2024-T3 (Fig. 1b), the porosities were generally significantly higher, suggesting that there were significant nucleation problems for these substrates and/or coating delamination occurring during the electrochemical testing as a result of poor adhesion. However, some of porosity values (for example, 56%) are unrealistically high to be considered as porosities, which might suggest that dissolution of the film during the measurements was occurring for such a large surface area to be seemingly bare. However, the trend was similar to the 100Cr6 substrates, where there was a general decrease in porosity with increasing film thickness. Again for the thermal ALD, the porosity of the films was higher than the plasma-enhanced method for the 10 nm thick films (∼56 and ∼30%, respectively) but equivalent for the 50 nm thick films (∼10%).

The temperature series was carried out for 10 nm thick films deposited by plasma-enhanced ALD (Fig. 2). For 100Cr6 steel, there was an almost linear decrease in the film porosity with increasing deposition temperature. It is known that Al_2O_3 films grown at lower temperatures tend to have lower densities, primarily due to the increased incorporation of OH groups.[20,22] Such densities leave the film prone to having a higher concentration of defects, therefore higher porosities, through which corroding media can travel. The plasma-enhanced method did, however, give a much lower film porosity (at 150°C) than the corresponding thermal ALD process, which is attributed mainly to the increased film density resulting from the higher reactivity provided by the plasma and the improved nucleation properties of the films. It should be noted that the thermal ALD process was not carried out at deposition temperatures lower than 150°C due to the long purge times required when using water; for example, Groner et al. reported necessary water purge times of 180 s at 33°C.[31] At 150°C, we found that only a 10 s water purge was necessary for thermal ALD, but for plasma-enhanced ALD, 2 s was sufficient for all temperatures.

For Al2024-T3 substrates, the opposite trend was observed, whereby the lowest deposition temperatures afforded the lowest film porosities (∼12%), which almost doubled at 150°C. However, in a similar manner to the 100Cr6, the porosity for the thermal ALD films was substantially higher than that for the plasma-enhanced ALD films deposited at 150°C.

TEM imaging.—Cross-sectional bright field TEM images showed that the Al_2O_3 deposited by both plasma-enhanced and thermal ALD were conformal on fine-ground Al2024-T3 (Fig. 3) and lapped 100Cr6 (Fig. 4). For the films deposited by plasma-enhanced ALD on Al2024-T3, the coating was present even in deep cracks in the substrate (Fig. 3), which shows that the O_2 plasma radicals can reach down trenches. Radicals formed in a plasma are known to

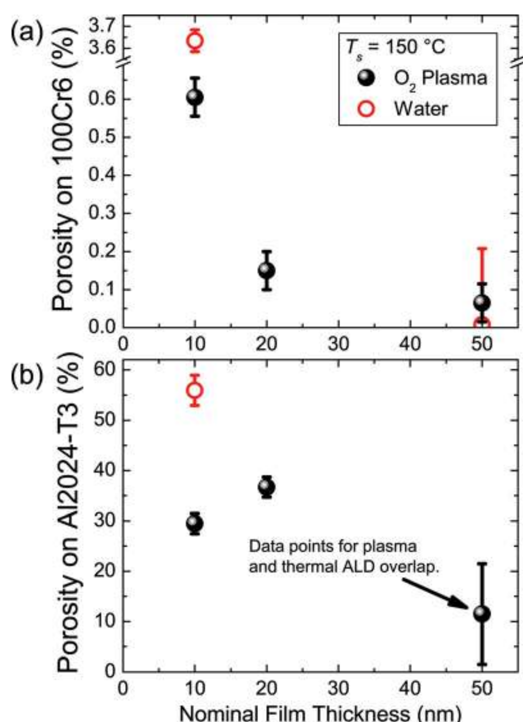

Figure 1. (Color online) Variation of film porosity as a function of film thickness for Al_2O_3 films deposited at 150°C on (a) lapped 100Cr6 and (b) fine-ground Al2024-T3. Note the break in the vertical axis for 100Cr6.

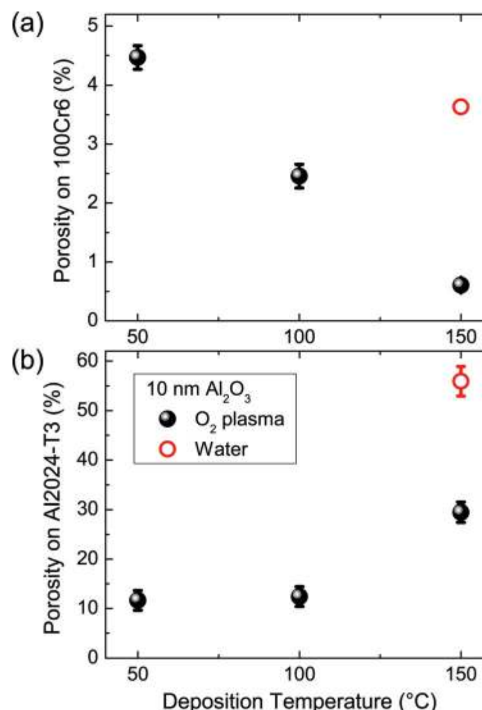

Figure 2. (Color online) Variation of film porosity as a function of deposition temperature for 10 nm thick Al_2O_3 films deposited by plasma-enhanced ALD on (a) lapped 100Cr6 and (b) fine-ground Al2024-T3. The porosity for films deposited by thermal ALD at 150 °C is given for comparison.

Downloaded 29 Mar 2011 to 131.155.151.8. Redistribution subject to ECS license or copyright; see http://www.ecsdl.org/terms_use.jsp

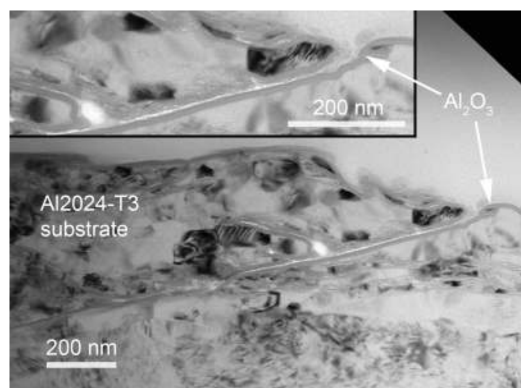

Figure 3. Bright-field TEM image of ∼20 nm Al_2O_3 deposited on Al2024-T3 by plasma-enhanced ALD at 150°C. Inset: close-up of the trench area.

recombine at surfaces, although oxygen radicals have a low recombination probability on metal oxides.[19,32] Therefore, it is likely that the native oxide on the Al2024-T3 allows the high aspect ratio trench to be coated.

For all thermal ALD samples, there was a void present (∼20 nm) between the substrate and coating (filled with glue used in the TEM preparation), suggesting that the Al_2O_3 film was not well adhered. The same was the case on 100Cr6 substrates (Fig. 4), where the film was separated from the substrate by ∼8 nm. The use of a plasma in the ALD process therefore has a beneficial influence on the adhesion of the film, which can be crucial for the coating's resistance to corrosion.

ToF-SIMS depth profiles.—Time-of-flight secondary ion mass spectroscopy studies were carried out on nominally 50 and 10 nm thick Al_2O_3 films on lapped 100Cr6 substrates in order to compare the plasma-enhanced and thermal ALD techniques. For the 50 nm thick samples (Fig. 5), there was no significant difference in the width of the interfacial region between the film and the substrate. This was not unexpected as this width is mostly governed by the roughness of the alloy surface, which causes shadowing effects during sputtering. Consequently, the slight differences in film thickness (Table I) between the plasma-enhanced and thermal ALD processes could not be resolved. In terms of the composition of the interfacial region, the signals of the FeO_2^- and CrO_2^- ions were slightly lower for the plasma-enhanced process, suggesting less contamination by the substrate oxide. However, the C^- and OH^- signals were comparable for both samples. In the bulk of the coatings there was a lower concentration of OH for the plasma-enhanced process in the later stages of deposition, which is a result of the higher reactivity of the

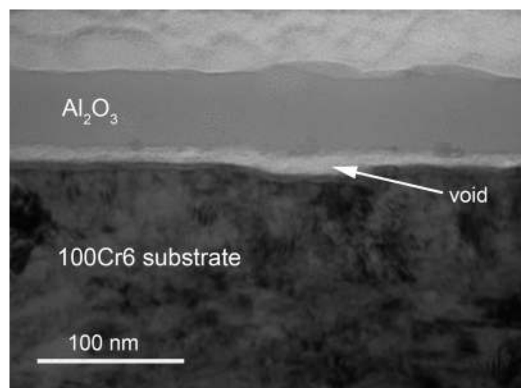

Figure 4. Bright-field TEM image of ∼55 nm Al_2O_3 deposited on 100Cr6 by thermal ALD at 150°C, showing a void filled with glue, from the TEM sample preparation, between the coating and the substrate.

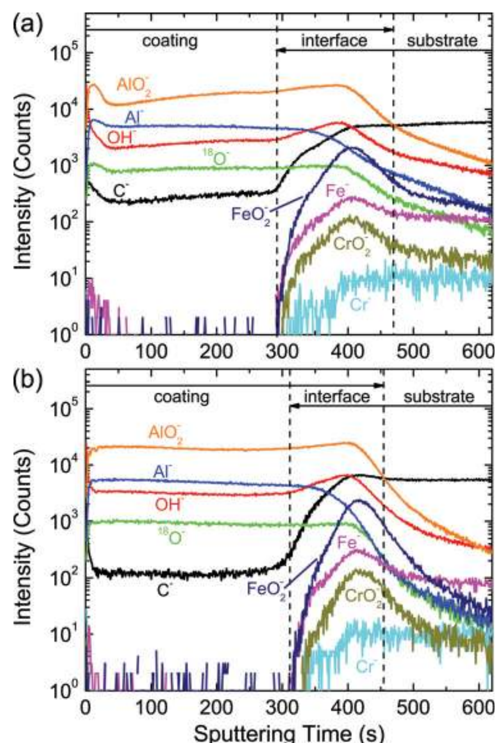

Figure 5. (Color online) ToF-SIMS depth profiles for 50 nm Al_2O_3 deposited at 150°C on 100Cr6 using (a) plasma-enhanced ALD and (b) thermal ALD.

plasma than water in the ALD process, causing film densification when the influence of interfacial contamination decreased. Film densification has been verified by Rutherford backscattering data on Al_2O_3 films, which has shown that films with lower OH concentrations have a higher density, and that films deposited by plasma-enhanced ALD are slightly denser than those deposited by thermal ALD.[22] Our ToF-SIMS data show that this effect is more sensitive away from the interfacial region. However, the presence of OH in the films is not necessarily detrimental to the coating efficiency since the lowest porosity was obtained with the 50 nm thick thermal ALD sample (which contained the more OH in the bulk of the coating). A similar trend has been observed in the use of Al_2O_3 as a protective coating for organic LEDs,[28] where the films containing more OH (which were deposited by plasma-enhanced ALD at room temperature) exhibited better moisture-barrier properties than films deposited at higher temperatures.

Regarding the coating surface, Fig. 6 shows that OH was present further below the surface for the plasma-enhanced ALD samples (up to ∼30 s sputtering) than for the thermal ALD sample (∼10 s sputtering), although the overall concentration of OH in the former was lower. This surface variation appears to be related to the AlO_2^- ion profile (Fig. 5), which shows a hump in the same near-surface region of the plasma-enhanced ALD sample, suggesting a deeper penetration of surface hydroxylation. This could be due to environment-induced modifications occurring during ex situ transfer for sample analysis. It is likely that this is promoted by the higher density of reactive surface sites on the plasma-enhanced ALD samples compared with those deposited by thermal ALD. A higher density of reactive surface groups is a characteristic of plasma-enhanced ALD and is one of the main contributing factors to the higher growths per cycle obtained.[21]

For the 10 nm thick samples, the difference between the two deposition methods is significantly more prominent (Fig. 7). For the film deposited by plasma-enhanced ALD, a sputtering time of ∼400 s was needed to reach the interface, whereas for thermal ALD, only 110 s was required (both of these samples were analysed with the same

Downloaded 29 Mar 2011 to 131.155.151.8. Redistribution subject to ECS license or copyright; see http://www.ecsdl.org/terms_use.jsp

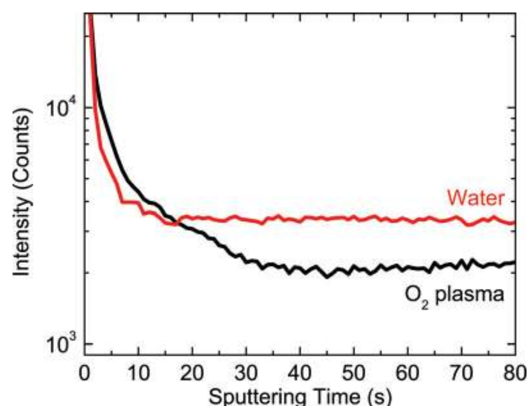

Figure 6. (Color online) ToF-SIMS depth profiles for the OH^- species at the surface of the 50 nm thick Al_2O_3 films deposited by plasma-enhanced (O_2 plasma) and thermal (water) ALD at 150°C.

sputtering target Cs^+ ion current density). This is not due to differing film thicknesses, as the results from the SE measurements (Table I) were very similar, but it suggests that the film deposited by thermal ALD was significantly less dense and, consequently, had a markedly higher sputtering yield. This is likely to be related to the better nucleation afforded by the use of a plasma as a co-reactant, which is also confirmed by the porosity results, therefore leading to denser films in the initial stages of growth. This densification is also supported by the slightly higher intensity of the Al^-, $^{18}O^-$ and AlO_2^- ion profiles in the bulk of the plasma-enhanced coating when compared with the thermal process. In both cases, the coating contained OH and C originating from environmental contamination and/or from incomplete removal of the precursors used for deposition. The OH and C signals were lower for the plasma-enhanced sample, which is also indicative of a denser Al_2O_3 layer that is less sensitive to environment-induced modifications. The non-uniform ion profiles obtained for the thermal ALD film are a consequence of the higher sensitivity of this sample to environmental contamination.

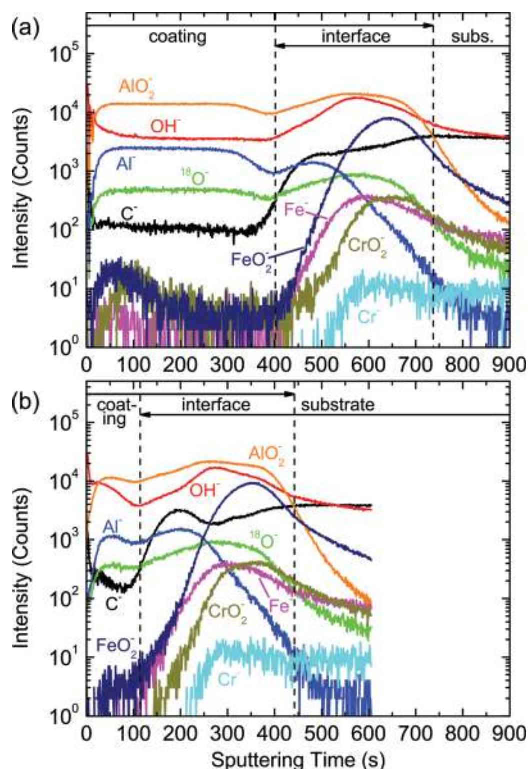

Figure 7. (Color online) ToF-SIMS depth profiles for 10 nm Al_2O_3 deposited at 150°C on 100Cr6 using (a) plasma-enhanced ALD and (b) thermal ALD.

NSS tests.— A thickness series, including films of nominally 10, 20 and 50 nm, was carried out on lapped (Fig. 8) and fine-ground (not shown) 100Cr6 steel. Where the Al_2O_3 thickness was nominally 10 nm, significant rust was visible on all samples after 2 h NSS testing. A slight improvement was observed on increasing the layer thickness to 20 nm as, despite there being a substantial amount of visible corrosion, less rust was observed after 2 h than on the 10 nm sample. At 50 nm, there was a clear improvement in the corrosion resistance, as the films were generally stable up to 4 h under NSS conditions. However, some slight corrosion was observed in specific areas, which is likely to be the result of defects in the film. For the temperature series (10 nm thick films deposited by plasma-enhanced ALD, not shown), there was no significant difference between the visible corrosion resistance of the films deposited at all temperatures. Also for the 10 nm thick films, there was no clear difference in the quantity of rust observed for thermal and plasma-enhanced ALD, whereas for the 50 nm thick films, less rust was observed for the plasma-enhanced samples. The surface finish of the substrates also made no clear difference according to the NSS tests. Our coated substrates showed more corrosion within 24 h NSS testing than the nearest equivalent coating, which was ~3 μm NbO_xN_y on 100Cr6 steel.[33] However, this is not unexpected as the thickness of our ALD was two orders of magnitude lower. Further comparison of NSS tests is difficult, as most procedures are carried out for 168 h or more before the quantity of rust is evaluated.

For the Al2024-T3 substrates (Fig. 9), a small number of corrosion spots were observed after 2 h NSS testing, but significant rusting did not occur until after 24 h. The film thickness, again, had some influence in the degree of corrosion protection, as the 50 nm thick films showed the most resistance. The deposition temperature did not make a visible difference to the amount of corrosion seen (not shown) and the difference between plasma-enhanced and thermal ALD was not so significant. It should be noted that the Al2024-T3 substrates themselves are more resistant to corrosion than 100Cr6. Consequently, direct comparisons between the NSS results of the coated metal substrates are difficult to make. Therefore, using this method, it was not possible to ascertain whether the Al_2O_3 coatings provided the same level of corrosion protection on Al2024-T3 as they did on 100Cr6.

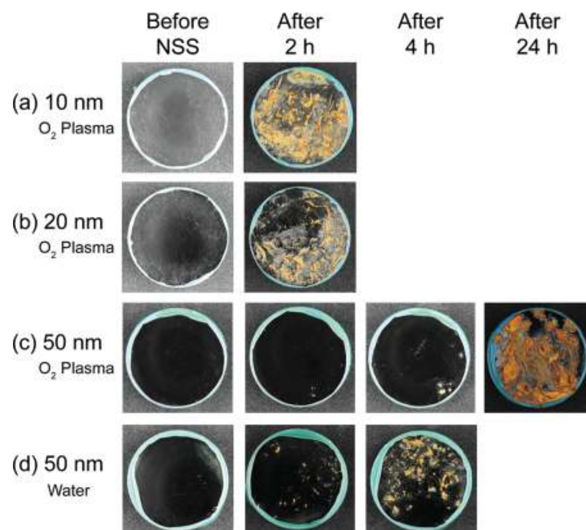

Figure 8. (Color online) NSS test results for lapped 100Cr6 samples coated at 150°C in (a) 10, (b) 20 and (c) 50 nm thick Al_2O_3 deposited by plasma-enhanced ALD and (d) 50 nm Al_2O_3 deposited by thermal ALD.

Downloaded 29 Mar 2011 to 131.155.151.8. Redistribution subject to ECS license or copyright; see http://www.ecsdl.org/terms_use.jsp

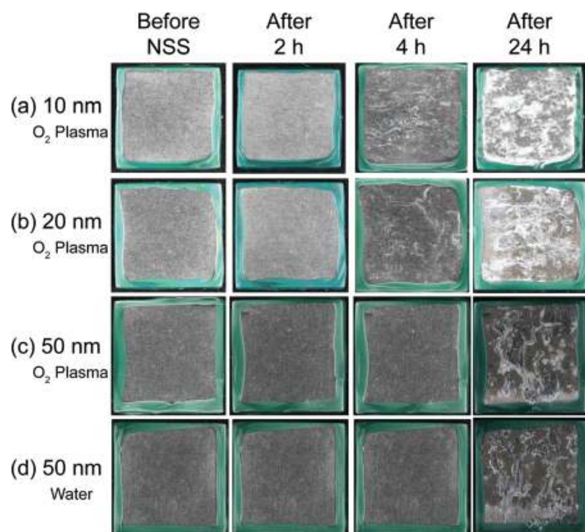

Figure 9. (Color online) NSS test results for fine-ground Al2024-T3 samples coated at 150°C in (a) 10, (b) 20 and (c) 50 nm Al_2O_3 deposited by plasma-enhanced ALD and (d) 50 nm Al_2O_3 deposited by thermal ALD.

Generally, the porosity of the films correlated well with the NSS results for both alloys, in that the thicker films were the least porous and provided the best corrosion protection. However, there were some discrepancies between the two techniques, whereby the porosity values for the 50 nm thick plasma-enhanced and thermal films were very similar yet the films deposited by plasma-enhanced ALD showed slightly better corrosion resistance. Also, the porosity data show a dependence on deposition temperature, whereas the NSS tests showed no change. This could be a feature of the measurement techniques themselves, as the CV measurements were taken in deaerated solutions, whereas, for the NSS tests, no special effort was made to exclude air, which could allow for faster corrosion.

Conclusions

10–50 nm thick Al_2O_3 thin films were applied to 100Cr6 steel and Al2024-T3 aluminium substrates as coatings for corrosion protection. The uncoated surface fraction determined from CV measurements showed that films deposited by plasma-enhanced ALD at 150°C were the least porous on 100Cr6, whereas on Al2024-T3 the films deposited at 50°C were the least porous. On both substrates, the 50 nm thick films had the best sealing performance, reaching a porosity lower than 0.5% on the 100Cr6 substrate. At 150°C, the plasma-enhanced ALD and thermal ALD films were approximately equivalent where the nominal thickness was 50 nm; however, for the 10 nm thick films, the plasma-enhanced method gave the lowest porosity because of better film nucleation in this case.

The improved nucleation by plasma-enhanced ALD was corroborated by cross-sectional TEM images, which showed that the 10 nm thick films deposited by thermal ALD were separated from the substrate, suggesting poor adhesion, whereas no void was observed for the films deposited using plasma-enhanced ALD. For the 50 nm thick films, ToF-SIMS depth profiles showed that the OH concentration was lower in the bulk of the films deposited by plasma-enhanced ALD than in those by thermal ALD. For the plasma-enhanced films, the OH concentration decreased with increasing film thickness, as the influence of the OH-contaminated buried film-substrate interface was reduced. The surface OH concentration was higher for the plasma-enhanced films as a result of a higher density of reactive sites, which promoted surface hydroxylation from ambient moisture over time. For the 10 nm thick films, the difference was more substantial, with the thermal ALD films requiring a shorter sputtering time to reach the film-substrate interface, confirming that the films deposited by plasma-enhanced ALD were significantly denser at this thickness.

Neutral salt spray tests confirmed that the thickest films gave the best corrosion resistance (>4 h) and that the films deposited by plasma-enhanced ALD offered longer protection than those deposited by thermal ALD. There was no significant difference observed for the 10 nm thick films deposited at different temperatures. Overall, the application of Al_2O_3 thin films to industrial alloys improved their resistance to corrosion. For the thicker (50 nm) films, the material deposited by both ALD techniques provided the most protection, with the films deposited by plasma-enhanced ALD showing the smallest quantity of rust after 4 h NSS testing. For the thinner (10 nm) films, plasma-enhanced ALD gave films with a lower porosity and better nucleation behaviour, showing that plasma-enhanced ALD is a promising method with which to deposit ultra-thin films for the sealing and corrosion protection of precision parts.

Acknowledgments

The research leading to these results has received funding from the European Community's Seventh Framework Programme (FP7/2007-2013) under grant agreement number CP-FP213996-1 (CORRAL). The authors thank W. Keuning, C. A. A. van Helvoirt, J. J. A. Zeebregts, and M. J. F. van de Sande for their technical assistance, support and advice.

Eindhoven University of Technology assisted in meeting the publication costs of this article.

References

1. R. Bayón, A. Igartua, X. Fernández, R. Martínez, R. J. Rodríguez, J. A. García, A. de Frutos, M. A. Arenas, and J. de Damborenea, *Tribol. Int.*, **42**, 591 (2009).
2. J. E. Gray and B. Luan, *J. Alloys Compd.*, **336**, 88 (2002).
3. H.-C. Lee, Y.-H. Hwang, and T.-G. Kim, *Eng. Failure Anal.*, **10**, 77 (2003).
4. G. Bierwagen, R. Brown, D. Battocchi, and S. Hayes, *Prog. Org. Coat.*, **67**, 195 (2010).
5. A. Akhtar, J. Y. Wong, G. S. Bhuyan, C. T. Webster, D. Kung, L. R. Gambone, N. Neufeld, and W. J. Brezden, *NDT & E Int.*, **25**, 115 (1992).
6. J. H. Smith, M. D. Rana, and C. Hall, *J. Pressure Vessel Technol.*, **125**, 177 (2003).
7. M. D. Rana and J. H. Smith, *J. Pressure Vessel Technol.*, **126**, 202 (2004).
8. D. Martínez, R. Gonzalez, K. Montemayor, A. Juarez-Hernandez, and G. Fajardo, *Wear*, **267**, 255 (2009).
9. N. L. Lee, G. B. Fisher, and R. Schulz, *J. Mater. Res.*, **3**, 862 (1988).
10. M. H. Ding, B. L. Wang, L. Li , and Y. F. Zheng, *Surf. Coat. Technol.*, **204**, 2519 (2010).
11. T. Goto, C.-Y. Guo, H. Takeya, and T. Hirai, *J. Mater. Sci.*, **27**, 233 (1992).
12. J. Perez-Mariano, K. H. Lau, E. Alvarez, R. Malhotra, M. Hornbostel, G. Krishnan, and A. Sanjuro, *Surf. Coat. Technol.*, **202**, 2794 (2008).
13. H.-R. Stock, H. Berndt, and P. Mayr, *Surf. Coat. Technol.*, **46**, 15 (1991).
14. J. R. Sobiecki, P. Mańkowski, and T. Wierzchoń, *Vacuum*, **68**, 105 (2003).
15. K. Gammer, M. Stoiber, J. Wagner, H. Hutter, R. Kullmer, and C. Mitterer, *Thin Solid Films*, **461**, 277 (2004).
16. S. M. George, *Chem. Rev.*, **110**, 111 (2010).
17. W. M. M. Kessels, S. B. S. Heil, E. Langereis, J. L. van Hemmen, H. C. M. Knoops, W. Keuning, and M. C. M. van de Sanden, *ECS Trans.*, **3**(15), 183 (2007).
18. H. B. Profijt, S. E. Potts, M. C. M. van de Sanden, and W. M. M. Kessels, *J. Vac. Sci. Technol. A*, Submitted.
19. W. M. M. Kessels, H. B. Profijt, S. E. Potts, and M. C. M. van de Sanden, *Atomic Layer Deposition of Nanostructured Materials*, Wiley-VCH, Weinheim, Germany, In press.
20. S. E. Potts, W. Keuning, E. Langereis, G. Dingemans, M. C. M. van de Sanden, and W. M. M. Kessels, *J. Electrochem. Soc.*, **157**, P66 (2010).
21. E. Langereis, J. Keijmel, M. C. M. van de Sanden, and W. M. M. Kessels, *Appl. Phys. Lett.*, **92**, 231904 (2008).
22. J. L. van Hemmen, S. B. S. Heil, J. H. Klootwijk, F. Roozeboom, C. J. Hodson, M. C. M. van de Sanden, and W. M. M. Kessels, *J. Electrochem. Soc.*, **154**, G165 (2007).
23. R. Matero, M. Ritala, M. Leskelä, T. Salo, J. Aromaa, and O. Forsén, *J. Phys. IV*, **9**, 493 (1999).
24. X. Du, K. Zhang, K. Holland, T. Tombler, and M. Moskovits, *Appl. Opt.*, **48**, 6470 (2009).
25. S.-H. K. Park, J. Oh, C.-S. Hwang, J.-I. Lee, Y. S. Yang, and H. Y. Chu, *Electrochem. Solid-State Lett.*, **8**, H21 (2005).
26. M. D. Groner, S. M. George, R. S. McLean, and P. F. Carcia, *Appl. Phys. Lett.*, **88**, 051907 (2006).
27. A. P. Ghosh, L. J. Gerenser, C. M. Jarman, and J. E. Fornalik, *Appl. Phys. Lett.*, **86**, 223503 (2005).

Downloaded 29 Mar 2011 to 131.155.151.8. Redistribution subject to ECS license or copyright; see http://www.ecsdl.org/terms_use.jsp

28. E. Langereis, M. Creatore, S. B. S. Heil, M. C. M. van de Sanden, and W. M. M. Kessels, *Appl. Phys. Lett.*, **89**, 081915 (2006).
29. E. Langereis, S. B. S. Heil, H. C. M. Knoops, W. Keuning, M. C. M. van de Sanden, and W. M. M. Kessels, *J. Phys. D: Appl. Phys.*, **42**, 073001 (2009).
30. W. Tato and D. Landolt, *J. Electrochem. Soc.*, **145**, 4173 (1998).
31. M. D. Groner, F. H. Fabreguette, J. W. Elam, and S. M. George, *Chem. Mater.*, **16**, 639 (2004).
32. H. C. M. Knoops, E. Langereis, M. C. M. van de Sanden, and W. M. M. Kessels, *J. Electrochem. Soc.*, **157**, G241 (2010).
33. M. Fenker, H. Kappl, P. Carvalho, and F. Vaz, *Thin Solid Films*, **519**, 2457 (2011).

Downloaded 29 Mar 2011 to 131.155.151.8. Redistribution subject to ECS license or copyright; see http://www.ecsdl.org/terms_use.jsp